Int. J. Heat Mass Transfer. Vol. 31, No. 9, pp. 1923–1932, 1988
Printed in Great Britain

0017–9310/88 $3.00 + 0.00

Thermosolutal convection in a floating zone: the case of an unstable solute gradient

JAYATHI Y. MURTHY and PETER LEE
Department of Mechanical and Aerospace Engineering, Arizona State University, Tempe, AZ 85287, U.S.A.

(*Received* 5 *October* 1987 *and in final form* 22 *February* 1988)

Abstract—The influence of laminar thermosolutal convection on solute segregation and heat transfer in the floating zone crystal growth of a dilute binary alloy is considered. The solute gradient is assumed to be destabilizing, and the thermal gradient is assumed perpendicular to it. The evolution of non-linear states from the critical points predicted by linear theory is studied. For vanishing thermal Rayleigh numbers, two solutions, corresponding to upflow and downflow at the meniscus, are obtained. The presence of side heating establishes upflow as the preferential direction; the downflow solution is found to persist for low thermal Rayleigh numbers. Flow and heat transfer for high thermal Rayleigh numbers are also computed.

INTRODUCTION

THE FLOATING zone process is a technique used in the containerless refinement of doped semi-conductor materials and binary alloys. In this process, a ring heater traverses a rod of alloy material to be purified, and melts a cylindrical zone in its path, as shown in Fig. 1. Refinement is achieved because the equilibrium concentration of dopant is greater in the melt than in the solid [1], corresponding to $k < 1$. At the melting interface, the dopant contained in the feed rod is absorbed completely into the melt, because it is more soluble in the melt than in the solid. At the freezing interface, however, all the dopant brought to the interface by convection and diffusion in the melt cannot be absorbed into the newly frozen crystal. Consequently, a dopant-rich layer forms in the melt at the freezing interface. An observer moving with the freezing interface would register this accumulation as an increase in dopant concentration with time. Eventually, a 'steady state' is reached when the dopant entering the zone at the melting interface exactly balances the dopant incorporated into the fresh crystal. No refinement takes place beyond this point.

In the absence of secondary convection in the melt, the segregation of solute is purely axial and varies exponentially, reaching a maximum at the freezing interface in steady state [1]. When the solute is lighter than the melt fluid and zone traverse is anti-parallel to gravity, a potential for the onset of convection exists beyond a critical solutal Rayleigh number, as with Rayleigh–Benard convection [2]. In addition, a horizontal temperature gradient is imposed because of meniscus heating by the ring heater. This gradient always induces natural convection. The purpose of this paper is to study the interaction of these two perpendicular gradients.

Most studies of double diffusive convection in crystal growth applications have focused on the problem of directional solidification of an ingot of binary alloy [3]. Here, a two-dimensional rectangular slug of melt fluid is solidified progressively from one end, with temperature and concentration gradients parallel to the direction of zone traverse. The thermal gradient is stabilizing, whereas the solute gradient is not. Much attention has been paid to the morphological stability of the freezing interface [4–8]. Analysis of a lead–tin system in ref. [5] showed that the coupling between convective and morphological instabilities is weak due to the great separation of the critical wave numbers. Consequently, Hurle *et al.* [6] examined the linear stability of solutal convection in the absence of morphological effects, i.e. in a melt with a planar interface. The critical solutal Rayleigh numbers computed were found to be low enough to suggest that solutal convection is the norm rather than the exception during directional solidification. McFadden and co-workers [9, 10] have examined numerically the flow transitions that occur during directional solidification of a binary alloy by assuming a planar interface. Steady-state solutions are found for solutal Rayleigh numbers about four times critical; beyond this, a transition to time periodic flows occurred and, finally, aperiodic flows.

The problem addressed by this work involves a somewhat different arrangement of driving forces, and finds many similarities with thermoconvective instability in bounded cylindrical layers heated from below. A very large number of studies for cylinders with either insulating or perfectly conducting side walls and rigid or shear-free boundaries is available in the literature [11–17]. Liang *et al.* [11] used a finite difference technique to study the axisymmetric flow of a fluid with a temperature-dependent viscosity. For aspect ratios near unity, the flow structure consists of a single roll filling the entire cylinder. Two solutions are found, corresponding to either upflow or downflow at the vertical axis of the cylinder. For constant fluid properties, these solutions are reflections of each other about the horizontal midplane of the cylinder. The onset of convection in a cylindrical layer of fluid

NOMENCLATURE

A	aspect ratio, L/d
c_0	solute concentration in feed rod
C	dimensionless solute concentration
d	radius of disk
D	diffusion coefficient for solute in melt
$\mathbf{e}_z$	unit vector in z-direction
g	acceleration due to gravity
$\mathbf{J}$	Jacobian matrix, equation (9)
k	equilibrium segregation coefficient
k_c	conductivity of melt fluid
L	length of zone, Fig. 1
$\mathbf{M}$	load matrix, equation (8)
Nu	local Nusselt number, equation (5)
$\overline{Nu}$	average Nusselt number, equation (5)
P	dimensionless pressure, scaled to $\rho\alpha^2/d^2$
Pe	Peclet number, $V_{in}d/D$
Pr	Prandtl number, ν/α
q	heat flux into zone at meniscus
r	radial coordinate, Fig. 1
R	dimensionless radial coordinate, r/d
$\mathbf{R}$	vector of residues, equation (6)
Ra_M	solutal Rayleigh number, $[g\beta c_0((1-k)/k)(d^3/\nu D)]/Pe^3$
Ra_T	thermal Rayleigh number, $g\beta(qd/k_c)d^3/\nu\alpha$
Sc	Schmidt number, ν/D
t	time
T	temperature
T_i	temperature of solid–melt interfaces
$\mathbf{V}$	velocity vector with components V_r, V_z
V_{in}	velocity of zone traverse
V_r	dimensionless radial velocity, scales to α/d
V_z	dimensionless axial velocity, scaled to α/d
$\mathbf{X}$	solution vector
$\mathbf{X}'$	disturbance vector
z	axial coordinate, Fig. 1
Z	dimensionless axial coordinate, z/d.

Greek symbols

α	thermal diffusivity
θ	dimensionless temperature, $(T-T_i)/(qd/k_c)$
μ	dynamic viscosity
ν	kinematic viscosity
σ	eigenvalue, equation (8)
σ_s	surface tension
Ψ	dimensionless stream-function
Ψ_v	strength of main vortex.

Other symbols

∇	dimensionless gradient operator
∇^2	dimensionless Laplacian operator.

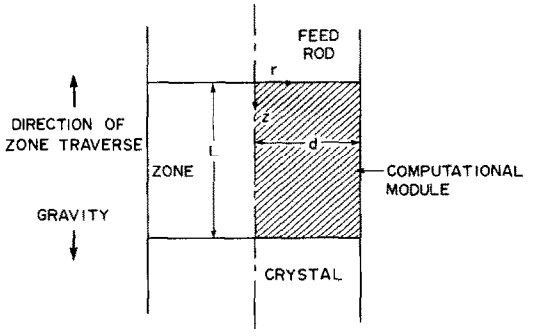

FIG. 1. The physical configuration.

bounded by rigid side walls and heated from below has been investigated by Charlson and Sani [12]. Axisymmetry is assumed, and upper and lower bounds to the critical Rayleigh numbers computed. Again the two solutions noted by Liang *et al.* are found. For small aspect ratios (L/d), multiple rolls in the radial direction are found past the critical point. The stability of axisymmetric flows to non-axisymmetric disturbances has been investigated in ref. [13]; it is found that a transition from axisymmetric to non-axisymmetric configurations may occur for certain ranges of aspect ratio near unity. Finite amplitude flows in the same geometry have been computed in ref. [14] using a Galerkin technique. Yamaguchi *et al.* [15] have investigated the same geometry using computer implemented perturbation techniques for tracking flow families and determining their stability.

The two-phase Rayleigh–Benard problem has been studied in using a Galerkin finite element technique, coupled with Newton iteration for the solution of the free melt–solid interface shape in ref. [18]. The flow is assumed driven by thermal gradients alone. Again, two solutions corresponding to upflow and downflow at the axis are found, but the bifurcation is not perfect; the deformation of the melt–solid interface breaks the symmetry between the two families. Cases with side heating, and top and bottom insulated boundaries corresponding to vertical Bridgeman growth, have also been considered in refs. [18, 19]; side heating is seen to make one family of flows inaccessible from the low Rayleigh number end.

In this study, the destabilizing gradient is the exponential axial variation of solute in the melt. The onset of convection and the subsequent evolution of finite amplitude flows is first computed for $Ra_T = 0$. The changes in flow structure as Ra_T is increased are then studied. Their influence on the overall heat transfer and solute distribution is examined.

FORMULATION

The geometry studied is that in Fig. 1. Invoking the Boussinesq approximation, the dimensionless equations governing the steady, axisymmetric, incom-

pressible motion of a Newtonian fluid in the zone may be written in the frame of reference of the heater as

$$\begin{aligned}
\nabla\cdot\mathbf{V} &= 0\\
\mathbf{V}\cdot\nabla\mathbf{V} &= -\nabla P + Pr\nabla^2\mathbf{V} - Ra_T\, Pr\,\theta\\
&\quad -(Ra_M\, Pe^3\, k/(1-k))\,(Pr^2/Sc)C\\
\mathbf{V}\cdot\nabla\theta &= \nabla^2\theta\\
\mathbf{V}\cdot\nabla C &= (Pr/Sc)\nabla^2 C. \qquad (1)
\end{aligned}$$

The boundary conditions on the velocity and temperature may be written as

$$V_r = 0, \quad V_z = Pe(Pr/Sc), \quad \theta = 0, \quad 0 \leqslant R \leqslant 1, \quad Z = 0, \quad A$$

$$V_r = \frac{\partial V_z}{\partial R} = \frac{\partial\theta}{\partial R} = 0, \quad 0 \leqslant Z \leqslant A, \quad R = 0$$

$$V_r = \frac{\partial V_z}{\partial R} = 0, \quad \frac{\partial\theta}{\partial R} = 1, \quad 0 \leqslant Z \leqslant A, \quad R = 1. \qquad (2)$$

The boundary conditions for solute transport are

$$\frac{\partial C}{\partial Z} = Pe(C-1), \quad Z = 0, \quad 0 \leqslant R \leqslant 1$$

$$\frac{\partial C}{\partial Z} = Pe(1-k)C, \quad Z = A, \quad 0 \leqslant R \leqslant 1$$

$$\frac{\partial C}{\partial R} = 0, \quad 0 \leqslant Z \leqslant A, \quad R = 0, 1. \qquad (3)$$

In the above formulation, the deformation of the free surface has been neglected; this assumption is valid for crystal growth applications with small capillary numbers ($\mu\alpha/\sigma_s$) and 90° contact angles between the solid and the meniscus. Marangoni convection has not been taken into account in order to focus on the natural convection process. A decoupling of morphological and convective instabilities allows the assumption of flat melt–solid interfaces if radial interface deformation due to the convective motion is assumed small. This latter assumption may be made if $qd/k_c \ll 1$, and typically applies to centimeter-scale zones. The influence of interfacial deformation on point of onset of convection has been found to be small in ref. [18]. The boundary conditions for solute transport assume that density of solid and melt are equal and that diffusion of solute in the feed rod is negligible. The parameters governing heat, mass and momentum transfer in this problem are the solutal Rayleigh number Ra_M, the thermal Rayleigh number Ra_T, the Prandtl number Pr, the Schmidt number Sc, the zone traverse Peclet number Pe, the aspect ratio A and the equilibrium segregation coefficient k.

The behavior of the secondary flow is quantified by extremum values of the stream-function defined as

$$\Psi = \int V_z R\,dR. \qquad (4)$$

Heat transfer behavior may be understood in terms of local and average Nusselt numbers at each interface, which are defined as

$$Nu = \left.\frac{\partial\theta}{\partial Z}\right|_{\text{interface}}$$

$$\overline{Nu} = 2\int_0^1 \left.\frac{\partial\theta}{\partial Z}\right|_{\text{interface}} R\,dR. \qquad (5)$$

NUMERICAL TECHNIQUE

Computation of finite amplitude flows

The governing equations and boundary conditions (equations (1)–(3)) are discretized using the control-volume scheme described in ref. [20] in conjunction with the power-law profile assumption also described in ref. [20]. Primitive variables are used, with a sequential solution of the continuity, momentum, energy and solute transport equations. Pressure–velocity coupling is handled using the SIMPLER algorithm [20]. This procedure yields a set of discrete algebraic equations which is solved iteratively, using a line-by-line application of the Thomas algorithm [20]. Successive substitutions are used to update the non-linear coefficients, with the under-relaxation procedure of ref. [20] to effect convergence of the iterative procedure.

Determination of the onset of convection

The discretized forms of equations (1)–(3) may be written as

$$\mathbf{R}(\mathbf{X}, Ra_M) = 0 \qquad (6)$$

where $\mathbf{R}$ is the vector of the residuals of the discrete algebraic equations. The critical value of the solutal Rayleigh number $Ra_{M,C}$, at the onset of convection, has been computed by examining the linear stability of equation (6). Perturbing equation (6) by a small disturbance yields

$$\mathbf{X}(t, Ra_M) = \mathbf{X}(Ra_M) + \mathbf{X}'\exp(\sigma t). \qquad (7)$$

Substituting equation (7) into equation (6) and subsequent linearization yields the eigenvalue problem

$$\mathbf{J}(\mathbf{X}, Ra_M)\mathbf{X}' = \sigma\mathbf{M}\mathbf{X}'. \qquad (8)$$

Here, $\mathbf{J}$ is the Jacobian matrix the elements of which are

$$J_{ij} = \frac{\partial R_i}{\partial X_j}. \qquad (9)$$

The linear stability of the base state $\mathbf{X}(Ra_M)$ may be completely determined by examining the eigenvalues of equation (8). However, the computation of eigenvalues for systems of several thousand equations is not feasible. Instead, the procedure adopted in ref. [15] is employed here. The locus of marginal stability may be found by setting both the real and imaginary parts of $\sigma = 0$. Thus, the problem of determining the onset of convection reduces to the determination of

those values of the solutal Rayleigh number for which the Jacobian **J** is singular. In this study, a simple bisection algorithm is used which determines the zeros of the determinant of **J** as a function of the solutal Rayleigh number. The determinant is computed from the L–U decomposition of **J**; the sparsity of **J** is exploited by the use of the sparse matrix package Y12M [21]. Computations of the onset of convection in the case of a rigid cylinder with bottom heating were performed to ascertain the accuracy of this method. Critical Rayleigh numbers computed using a 16×16 grid were within 5% of those obtained by Charlson and Sani [12]. For most aspect ratios, the results were within 2%.

The computations of finite amplitude flows were performed on a 30×30 non-uniform grid; computations on finer grids indicate that the strength of secondary cells and the average Nusselt number at the melting interface is accurate to 3%. The computation of critical Ra_M was performed on a 24×24 grid. For $Pe = 10$, $k = 0.1$, $A = 1.0$ and $Sc = 5.0$, the critical Rayleigh number changes by a maximum of 4% compared with those on a 30×30 grid. For most computations, the change is less than 2%. Further grid refinement requires more memory than available; the pivoting practices used in the package Y12M result in relatively dense L–U decompositions and memory requirements increase rapidly with grid refinement.

An aspect ratio $A = 1.0$ is assumed throughout this study. The computation of flow and heat transfer in the non-linear regime is restricted to $0 < Ra_T < 10^6$, $0 < Ra_M < 4.5 \times 10^7$, $Sc = 5.0$, $k = 0.1$ and $Pe = 1.0$. Two values of the Prandtl number are considered, $Pr = 0.01$ and 1.0.

RESULTS

Flows near $Ra_M = Ra_{M,C}$

The linear stability problem is governed by the Peclet number, the Schmidt number, the aspect ratio and the equilibrium segregation coefficient k. The base state is described by

$$V_r = 0, \quad V_z = Pe(Pr/Sc)$$

$$C(Z) = 1 + \left(\frac{1-k}{k}\right)\exp[Pe(Z-A)]. \qquad (10)$$

The variation of the first critical solutal Rayleigh number with Peclet number is presented in Figs. 2(a) and (b), the former being plotted for $Pe < 1$ and the latter for $Pe > 1$. In Fig. 2(a), the ordinate is $(Ra_{M,C}\ Pe^3)$, and represents a rescaling appropriate for the low Pe limit. The critical Rayleigh number is obtained for five sets of parameters, $Sc = 5.0, k = 0.1$, 0.2, 0.3, and $k = 0.1$, $Sc = 1.0$, 10.0. It is seen from Fig. 2(a) that all five curves collapse onto a single curve when scaled in this way. In Fig. 2(b), again, the critical Ra_M based on the boundary layer thickness is found to be primarily a function of the Peclet number for $Pe < 4$ or so. Beyond this, the strength of the opposing flow due to zone translation ($= Pe/Sc$) begins to exert a significant influence. As a result, the critical Rayleigh number is no longer a function of Pe alone.

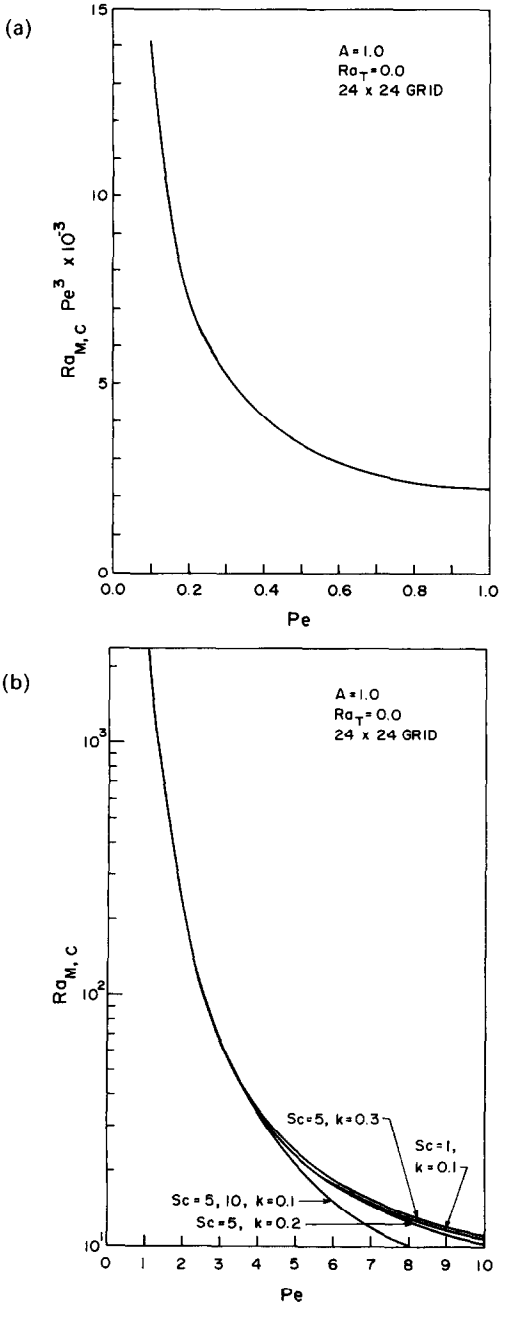

FIG. 2. Variation of the critical solutal Rayleigh number with Peclet number for $A = 1.0$ for: (a) $Pe < 1$; (b) $Pe > 1$.

The flows evolving from the first critical Rayleigh number are presented in Fig. 3. Here, the strength of the secondary flow is plotted vs the solutal Rayleigh number. Contours of the stream-function, temperature and solute concentration for $Ra_M = 4.5 \times 10^4$ are drawn in Fig. 4. Two families of flows are seen to evolve from the point of bifurcation, and correspond to upflow and downflow at the meniscus. The exist-

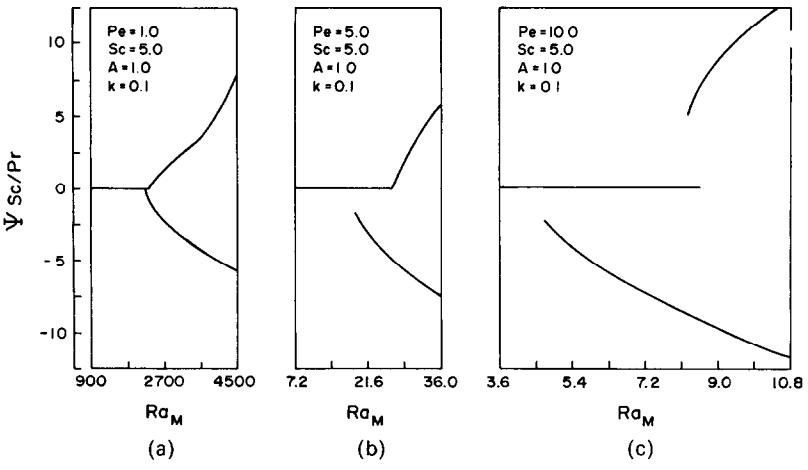

FIG. 3. Details of the bifurcation at $Ra_M = Ra_{M,C}$ with $A = 1.0$, $k = 0.1$, $Sc = 5.0$.

ence of these two families of solutions in the problem of thermoconvective stability in cylindrical enclosures has been noted both experimentally and analytically [11]. As pointed out in ref. [11], the thermoconvective stability problem with fixed temperature conditions at $Z = 0$ and A and adiabatic side walls, has the property

$$\{V_r, -V_z, -\theta', R, 1-Z\}_{\text{downflow}} = \{V_r, V_z, \theta', R, Z\}_{\text{upflow}} \quad (11)$$

where

$$\theta' = \theta - Z.$$

In the problem considered in this paper, the boundary conditions on concentration at $Z = 0$ and A (equation (3)) destroy this reflective symmetry about the horizontal midplane, and the perfect bifurcation noted for the constant viscosity case in refs. [11, 15] is no longer found. For low Peclet numbers, the bifurcation is transcritical, with the downflow solution evolving subcritically in the vicinity of the bifurcation point and reaching a limit point in Ra_M as seen in Fig. 3(b); thereafter, the solution evolves towards increasing Rayleigh numbers. As the Peclet number is increased further, both branches initially evolve subcritically and reach a limit point in Ra_M, as in Fig. 3(c); beyond this both solutions evolve in the direction of increasing Rayleigh number. The Jacobian of the discrete algebraic equations becomes singular at limit points [22]; consequently, it is impossible to trace solution families through limit points unless special continuation procedures are adopted. In this study, the various solution branches were traced by regulating direction of recirculation of the initial guess. The initial subcritical evolution of the flow near the critical point could not be traced in this manner. Computations using the trivial solution as a guess invariably yielded trivial solutions; computations using guesses from runs with $Ra_M > Ra_{M,C}$ invariably yielded solutions on the same branch, but past the

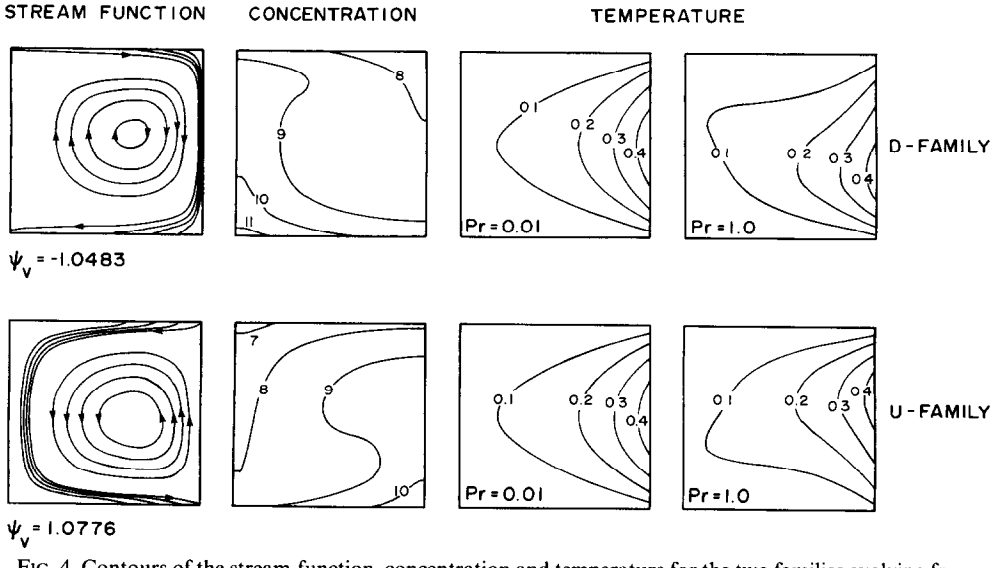

FIG. 4. Contours of the stream-function, concentration and temperature for the two families evolving from $Ra_M = Ra_{M,C}$, for $Ra_M = 4.5 \times 10^4$, $A = 1.0$, $k = 0.1$, $Sc = 5.0$ and $Pe = 1.0$.

subcritical limit point. Continuation procedures employing the pseudo-arc length parametrization of Keller [23] are required to trace the solution through limit points.

The $Pe = 1.0$ case is studied in greater detail in Figs. 5 and 6. With $Ra_T = 0$, the upflow solution is found to persist to at least a solutal Rayleigh number of 4.5×10^7. The downflow solution encounters a limit point at about $Ra_M = 3.6 \times 10^6$, and attempts to recover it using the iterative procedure described above always produce the upflow solution beyond this point. This behavior is quite different from that observed in ref. [15]; here, both upflow and downflow solutions encounter limit points, so that there are no stable two-dimensional solutions beyond the limit point. Periodic motions of the type noted in ref. [10] cannot be found using a steady procedure; however, the transient-like under-relaxation scheme used [20] always led to a converged steady-state solution.

The influence of a non-zero thermal Rayleigh number is to rupture the connectivity between the two families of flows, so that only the upflow solution is accessible from the low Ra_M end. The trivial solution described by equation (10) is no longer a solution to the thermal boundary conditions; instead, the strength of secondary convection increases gradually from a non-zero value at $Ra_M = 0$, with upflow at the meniscus. This behavior has been noted elsewhere, for example, in the case of thermal convection in a box heated from below, with imperfectly insulated side walls [24, 25]. The downflow solution is now isolated from this family of flows, and becomes increasingly so as Ra_T is increased. The behavior for $Pr = 1.0$ is presented in Fig. 5. For $Ra_T = 10^3$, the downflow solution exists for $1.422 \times 10^4 < Ra_M < 3.9 \times 10^6$; for $Ra_T = 2 \times 10^3$, the solution is found for $6.73 \times 10^4 < Ra_M < 3.9 \times 10^6$. For $Ra_T = 10^4$, the solution is restricted to $9.6 \times 10^5 < Ra_M < 3.9 \times 10^6$. For $Ra_T = 10^5$, the entire downflow solution branch is unstable. Similar behavior is seen for $Pr = 0.01$ in Fig. 6, albeit for much lower thermal Rayleigh numbers. Thus, for $Ra_T = 10$, the downflow solution exists for $1.7 \times 10^4 < Ra_M < 3.6 \times 10^6$; for $Ra_T = 20$, it is found in the range $9.63 \times 10^4 < Ra_M < 3.6 \times 10^6$. By $Ra_T = 100$, downflow is found only in the narrow range $2.2 \times 10^5 < Ra_M < 4.1 \times 10^6$. The dominance of thermal convection over solutal convection for $Pr/Sc \ll 1$ is evident from the V_z momentum equation in equations (1).

Attempts to compute flows corresponding to higher eigenmodes did not yield stable steady solutions. Similar behavior was noted in ref. [15] for the case of a rigid cylinder heated from below.

Thermosolutal convection at high Ra_T

The evolution of the family of solutions corresponding to upflow at the meniscus was traced up to $Ra_T = 10^6$ for $A = 1.0$, $Sc = 5.0$, $Pe = 1.0$ for $Pr = 0.01$ and 1.0, with $0 < Ra_M < 4.5 \times 10^7$. Stable steady solutions were always found in this range of values. Contours of the stream-function, temperature and solute concentration are presented in Fig. 7 for $Pr = 0.01$, and in Fig. 8 for $Pr = 1.0$. For $Pr = 0.01$, the strength of the secondary flow, Ψ_v, is seen to increase as the thermal Rayleigh number increases.

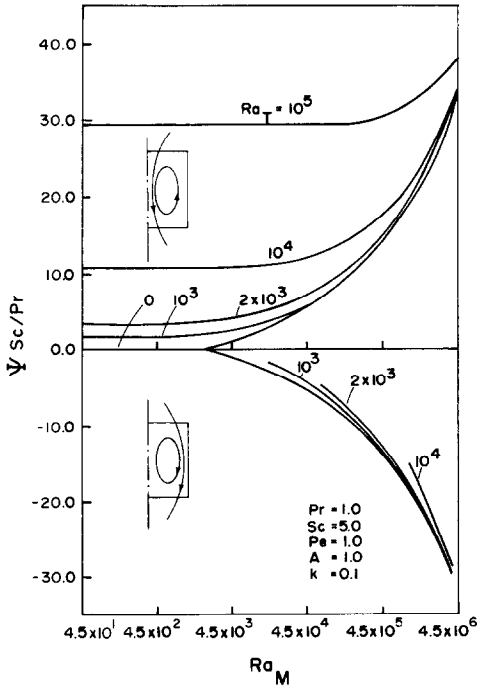

FIG. 5. The influence of Ra_T on the bifurcation at $Ra_M = Ra_{M,C}$ for $Pr = 1.0$, $A = 1.0$, $k = 0.1$, $Sc = 5.0$ and $Pe = 1.0$.

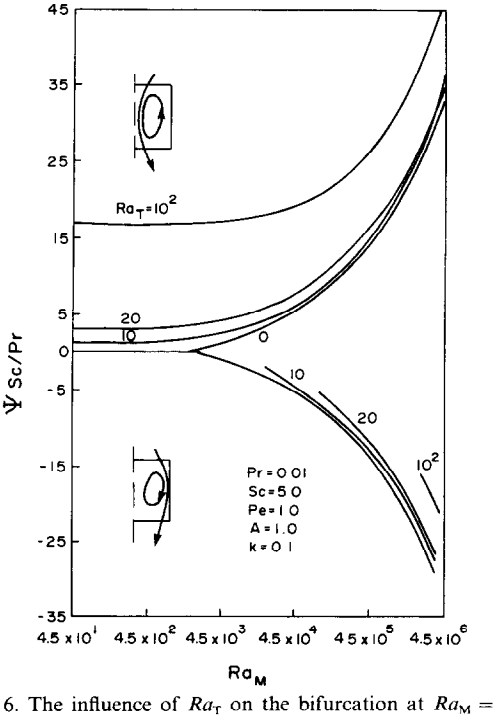

FIG. 6. The influence of Ra_T on the bifurcation at $Ra_M = Ra_{M,C}$ for $Pr = 0.01$, $A = 1.0$, $k = 0.1$, $Sc = 5.0$ and $Pe = 1.0$.

The flow is viscosity-dominated at $Ra_T = 10^3$. By $Ra_T = 10^5$, two small recirculation bubbles appear, one near the axis and the other at the meniscus. Their strengths are Ψ_A and Ψ_M, respectively. The latter disappears when the Rayleigh number is increased to 10^6. The solute in the zone is well mixed by convection even for low Ra_T values. The temperature solution for $Ra_T = 10^3$ is the conduction solution and is symmetric about the horizontal mid-plane. As Ra_T is increased, heat supplied at the meniscus is delivered almost exclusively to the outer edge of the melting interface and the mean temperature of the melt and the maximum meniscus temperature are seen to fall. For $Pr = 1.0$, the secondary flow penetrates the melt to a greater extent, and is stronger. A tendency for the fluid to lift off the freezing interface is exhibited for high Ra_T. This appears to be a result of local thermal gradients set up by the impinging flow. The concentration field is less homogeneous for high Pr than for low Pr, and substantial radial segregation exists at the freezing interface for $Pr = 1.0$.

For the thermal boundary conditions specified in this paper, the heat supplied at the meniscus must equal the heat transfer to the melting and freezing interfaces. Thus, for an aspect ratio of unity, the average Nusselt numbers at the melting and freezing interfaces defined by equation (5) must always sum to two. The average Nusselt number at the melting interface is plotted vs the thermal Rayleigh number in Fig. 9. For $Ra_M = 0$, $\overline{Nu}$ increases with Ra_T, but the rate of rise is seen to decrease; it is expected that eventually, the curve for $\overline{Nu}$ will level off. As Ra_M is increased, the local heat transfer is increasingly skewed towards the outer edge, as seen in Figs. 10(a) and (b). The increasingly isothermal melt cannot sustain thermally driven convection; this leads to a decrease in secondary convection, and a more equitable distribution of interfacial heat transfer, which, in turn, tends to drive stronger thermoconvective flows. The net effect is that an optimum configuration is reached such that increases in Ra_T do not result in indefinitely large secondary motions. The same is true for pure solute-driven convection; increased mixing by the secondary flow tends to homogenize the melt and actually

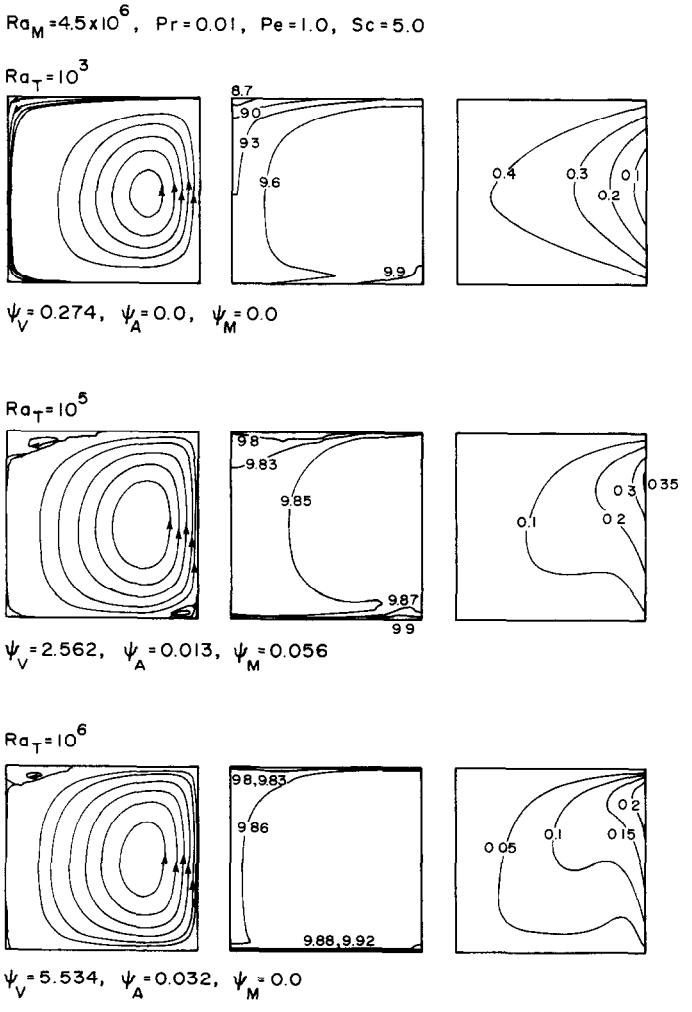

FIG. 7. Contours of the stream-function, concentration and temperature for $Pr = 0.01$, $Ra_M = 4.5 \times 10^6$, $A = 1.0$, $k = 0.1$, $Sc = 5.0$ and $Pe = 1.0$.

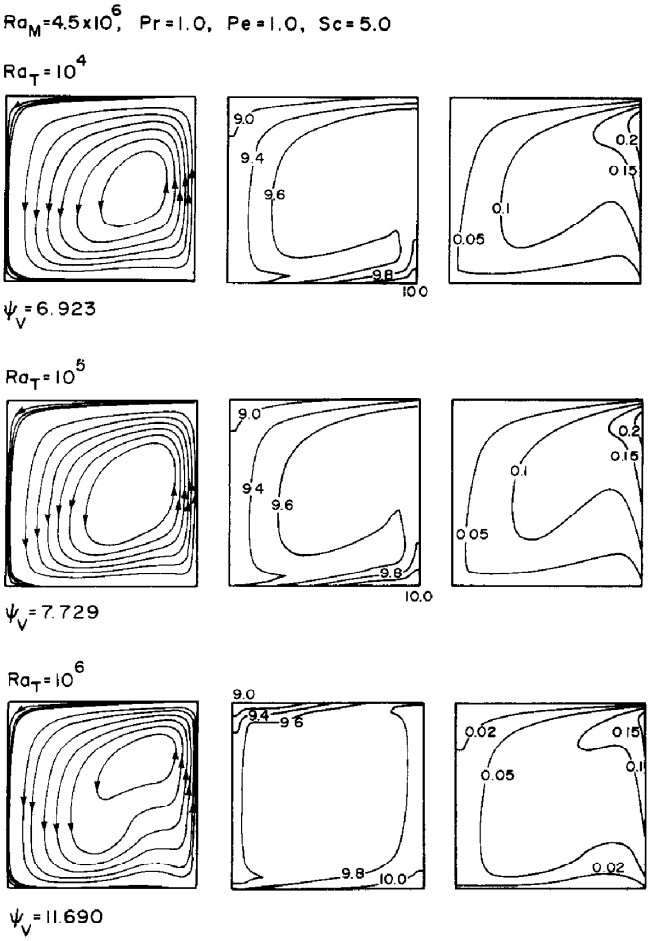

FIG. 8. Contours of the stream-function, concentration and temperature for $Pr = 1.0$, $Ra_M = 4.5 \times 10^6$, $A = 1.0$, $k = 0.1$, $Sc = 5.0$ and $Pe = 1.0$.

decreases the driving forces, which, in turn, leads to less mixing and larger concentration gradients. Thus, for $Ra_T = 10^3$, $Pr = 1.0$, the curves for the various Ra_M are seen to approach a constant $\overline{Nu}$ value. This tendency for the flow to regulate itself is clearly a result of the Neumann boundary conditions on temperature at the meniscus, and the solute boundary conditions, equations (3).

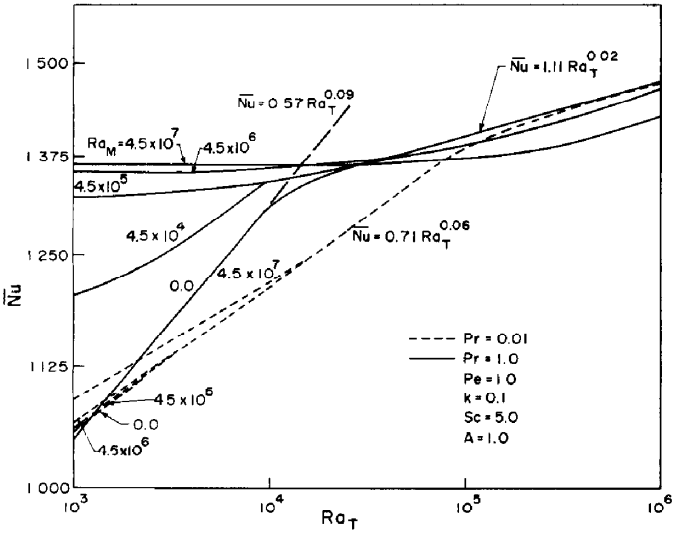

FIG. 9. The variation of the average Nusselt number at the melting interface with Ra_T for $A = 1.0$, $k = 0.1$, $Sc = 5.0$ and $Pe = 1.0$.

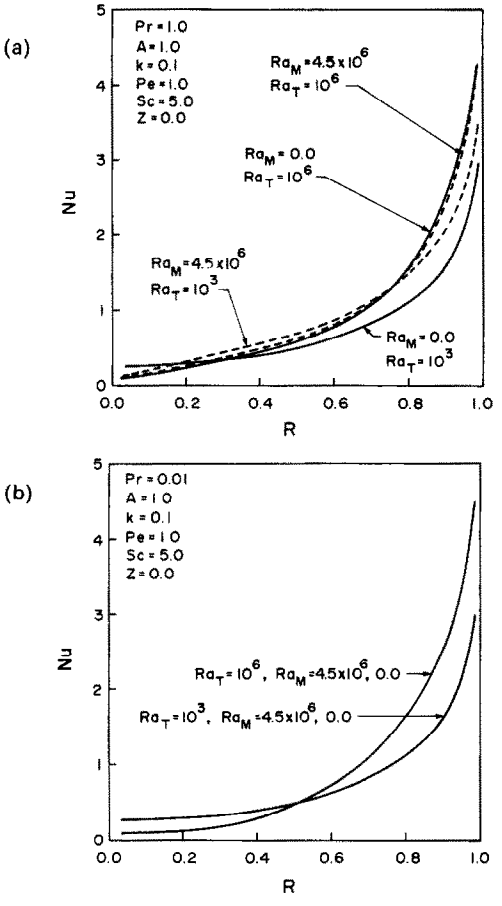

FIG. 10. The variation of local Nusselt number along the melting interface for $A = 1.0$, $k = 0.1$, $Sc = 5.0$ and $Pe = 1.0$ for: (a) $Pr = 1.0$; (b) $Pr = 0.01$.

Local and average heat transfer is seen to be nearly independent of Ra_M for $Pr/Sc \ll 1$ in the range of Ra_T considered. As seen in Fig. 8, the melt concentration is very nearly homogeneous even for $Ra_T = 10^3$, and has no effect on buoyant convection. Thus, for crystal growth applications, where Prandtl numbers of $O(10^{-2})$ are common, it appears that the flow is driven almost entirely by thermal convection unless

$$Ra_M \sim (Ra_T)(Sc/Pr)\left(\frac{1-k}{k}\right)\Big/ Pe^3$$

or greater.

CONCLUSIONS

Thermosolutal convection in a floating zone has been computed for two different Prandtl numbers. When the thermal Rayleigh number is zero, the onset of convection is computed as a bifurcation from the quiescent state. Two solutions, corresponding to upflow and downflow at the meniscus are found. For non-zero Ra_T, the upflow solution becomes the preferred family if computations commence from the zero Ra_M limit; the transition is gradual, i.e. there is no bifurcation. For high values of Ra_T, the heat transfer and the concentration field are largely independent of Ra_M if Pr/Sc is small.

The realization of the two families of solutions obtained in the computations is probably very difficult in practice. Even small values of the thermal Rayleigh number make the downflow solution inaccessible from the zero Ra_M end; specific experimental strategies are required to isolate the various solution branches. In practice, the steady-state solutions computed here are the culmination of an unsteady process in which the rates of development of the thermal, velocity and concentration boundary layers differ widely. For $Pe < 1$, and $Pr/Sc < 1$, thermal convection due to side heating will probably develop faster than the concentration boundary layer, and will determine the direction of the recirculation. The nature of the bifurcation itself may change if planar interfaces are not assumed. This study is restricted to low Peclet numbers of zone traverse; practical values vary widely, and may be as high as 10^2–10^3. For $Pe \gg 1$, the concentration boundary layer is $O(Pe^{-1})$ and is extremely difficult to resolve accurately. Nevertheless, the present study provides a basis for understanding the behavior of more complex problems.

No attempt has been made in this study to formally establish the stability of various solution branches. Preliminary attempts to duplicate the results of ref. [15] yielded only the stable solutions reported in that study; the unstable solutions traced by Chang and Brown could not be realized. As noted in ref. [20], the under-relaxation procedure employed in this study for the solution of the non-linear algebraic equations resulting from discretization is identical to the fully implicit procedure for solving unsteady problems. Each iteration is exactly equivalent to a time step for linear problems; the convergence of the iterative procedure to a solution is equivalent to the achievement of steady state. Numerical round-off imposes random disturbances on the flow; if these disturbances do not grow with iteration (time), convergence to a solution is achieved. In this respect, the numerical procedure employed here behaves like an experiment: only stable solutions may be physically realized.

Acknowledgement—This research was supported by National Science Foundation Grant CBT-8504917.

REFERENCES

1. W. G. Pfann, *Zone Melting*. Wiley, New York (1966).
2. S. Chandrasekhar, *Hydrodynamic and Hydromagnetic Stability*. Oxford University Press, London (1968).
3. M. E. Glicksman, S. R. Corriell and G. B. McFadden, Interaction of flows with the crystal–melt interface, *Ann. Rev. Fluid Mech.* **18**, 307–335 (1986).
4. W. W. Mullins and R. F. Sekerka, Stability of a planar interface during solidification of dilute binary alloy, *J. Appl. Phys.* **34**, 323–329 (1964).
5. S. R. Coriell, M. R. Cordes, W. J. Boettinger and R. F. Sekerka, Convective and interfacial instabilities during unidirectional solidification of a binary alloy, *J. Crystal Growth* **49**, 13–28 (1980).

6. D. T. J. Hurle, E. Jakeman and A. A. Wheeler, Hydrodynamic stability of the melt during solidification of a binary alloy, *Physics Fluids* **26,** 624–626 (1983)
7. D. R. Jenkins, Nonlinear analysis of convective morphological instability during solidification of a dilute binary alloy, *Physicochem. Hydrodyn.* **6,** 521–537 (1985).
8. G. W. Young and S. H. Davis, Directional solidification with buoyancy in systems with small segregation coefficient, *Phys. Rev.* **B34,** 3388–3396 (1986).
9. G. B. McFadden, R. G. Rehm, S. R. Coriell, W. Chuck and K. A. Morrish, Thermosolutal convection during directional solidification, *Metall. Trans.* **A15,** 2125–2137 (1984).
10. G. B. McFadden and S. R. Coriell, Thermosolutal convection during directional solidification. II. Flow transitions, *Physics Fluids* **3,** 659–671 (1987).
11. S. F. Liang, A. Vidal and A. Acrivos, Buoyancy-driven convection in cylindrical geometries, *J. Fluid Mech.* **32,** 619–624 (1968).
12. G. S. Charlson and R. L. Sani, Thermoconvective instability in a bounded cylindrical fluid layer, *Int. J. Heat Mass Transfer* **13,** 1479–1496 (1970).
13. G. S. Charlson and R. L. Sani, On thermoconvective instability in a bounded cylindrical fluid layer, *Int. J. Heat Mass Transfer* **14,** 2157–2160 (1971).
14. G. S. Charlson and R. L. Sani, Finite amplitude axisymmetric thermoconvective flows in a bounded cylindrical layer of fluid, *J. Fluid Mech.* **71,** 209–229 (1975).
15. Y. Yamaguchi, C. J. Chang and R. A. Brown, Multiple buoyancy-driven flows in a vertical cylinder heated from below, *Phil. Trans. R. Soc. Lond.* **A312,** 519–552 (1984).
16. C. A. Jones, D. R. Moore and N. D. Weiss, Axisymmetric convection in a cylinder, *J. Fluid Mech.* **73,** 353–388 (1976).
17. S. Rosenblat, Thermal convection in a vertical circular cylinder, *J. Fluid Mech.* **122,** 395–410 (1982).
18. C. J. Chang and R. A. Brown, Natural convection in steady solidification: finite element analysis of a two-phase Rayleigh–Benard problem, *J. Comp. Phys.* **53,** 1–27 (1984).
19. C. J. Chang and R. A. Brown, Radial segregation induced by natural convection and melt/solid interface shape in vertical Bridgeman growth, *J. Crystal Growth* **63,** 343–364 (1983).
20. S. V. Patankar, *Numerical Heat Transfer and Fluid Flow.* McGraw-Hill, New York (1980).
21. Z. Zlatev, J. Wasniewski and K. Schaumburg, Y12M: solution of large and sparse systems of linear algebraic equations. In *Lecture Notes in Computer Science*, Vol. 121. Springer, New York (1981).
22. M. Kubicek and M. Marek, *Computational Methods in Bifurcation Theory and Dissipative Structures.* Springer, New York (1983).
23. H. B. Keller, Numerical solution of bifurcation and nonlinear eigenvalue problems. In *Applications of Bifurcation Theory* (Edited by P. H. Rabinowitz), pp. 359–384. Academic Press, New York (1977).
24. P. Hall and I. C. Walton, The smooth transition to a convective regime in a two-dimensional box, *Proc. R. Soc. Lond.* **A358,** 199–221 (1977).
25. P. G. Daniels, The effect of distant sidewalls on the transition to finite amplitude Benard convection, *Proc. R. Soc. Lond.* **A358,** 173–197 (1977).

UNE ZONE FLOTTANTE EN CONVECTION THERMOSOLUTALE: CAS D'UN GRADIENT INSTABLE DE SOLUTE

Résumé—On considère l'influence de la convection thermosolutale laminaire sur la ségrégation du soluté et sur le transfert de chaleur dans la zone flottante pendant la croissance cristalline d'un alliage binaire dilué. Le gradient de soluté est supposé être déstabilisant et le gradient thermique lui est perpendiculaire. On étudie l'évolution des états non linéaires à partir des points critiques prédits par la théorie linéaire. Pour un nombre de Rayleigh thermique s'évanouissant, deux solutions sont obtenues qui correspondent pour un mouvement ascendant et descendant au ménisque. La présence d'un chauffage latéral établit le mouvement ascendant comme préférentiel; la solution descendante persiste pour les faibles nombres de Rayleigh. On calcule aussi l'écoulement et le transfert de chaleur pour les nombres de Rayleigh élevés.

KONVEKTION INFOLGE VON TEMPERATUR- BZW. KONZENTRATIONSGRADIENTEN IN EINEM STRÖMENDEN BEREICH: DER FALL EINES VERÄNDERLICHEN GRADIENTEN DES GELÖSTEN STOFFES

Zusammenfassung—Es wird der Einfluß der laminaren, durch Temperatur- und Konzentrationsgradienten getriebenen Konvektion auf die Abscheidung des gelösten Stoffes und den Wärmetransport für das Kristallwachstum im strömenden Bereich einer verdünnten, binären Mischung betrachtet. Der Gradient des gelösten Stoffes wird als destabilisierend angenommen, der Temperaturgradient soll senkrecht dazu stehen. Die Entstehung nicht-linearer Zustände vom kritischen Punkt aus, die die lineare Theorie voraussagt, wird betrachtet. Für verschwindende thermische Rayleigh-Zahlen erhält man zwei Lösungen, die einem aufwärts bzw. abwärts gerichteten Strom am Meniskus entsprechen. Eine seitlich vorhandene Beheizung führt bevorzugt zu aufwärts gerichteter Strömung; die Lösung für Abwärtsströmung bleibt für kleine thermische Rayleigh-Zahlen bestehen. Außerdem werden Strömung und Wärmetransport für große thermische Rayleigh-Zahlen berechnet.

ТЕРМОКОНЦЕНТРАЦИОННАЯ КОНВЕКЦИЯ В ЗОНЕ ФЛОТАЦИИ: СЛУЧАЙ НЕУСТОЙЧИВОГО ГРАДИЕНТА КОНЦЕНТРАЦИИ РАСТВОРЕННОГО ВЕЩЕСТВА

Аннотация—Рассматривается влияние ламинарной термоконцентрационной конвекции на выделение растворенного вещества и теплоперенос при росте кристалла в зоне флотации разбавленного бинарного сплава. Предполагается, что градиент концентрации растворенного вещества является дестабилизирующим фактором и что температурный градиент направлен перпендикулярно ему. Исследуется предсказанный линейной теорией процесс развития нелинейных состояний после критических точек. При стремящихся к нулю значениях теплового числа Рэлея получены два решения, соответствующие восходящему и нисходящему потокам в области мениска. Боковой нагрев вызывает в основном восходящий поток. Найдено, что при малых тепловых числах Рэлея наблюдается нисходящий поток. Рассчитаны также течение и теплоперенос при больших значениях теплового числа Рэлея.